 https://doi.org/10.3311/PPci.37309

Periodica Polytechnica Civil Engineering, 69(1), pp. 280–292, 2025

Modeling the Segmental Lining Behavior Using an Analytical Segmental Joint Model

Fan Yang[1,2], Guang Liu[1*], Wu Liu[1], Kang Liu[1], Yan-qiao Wang[1], Huayan Yao[1]

[1] School of Civil and Hydraulic Engineering, Hefei University of Technology, Tunxi Road 193., 230009 Hefei, China
[2] Anhui Province Key Laboratory of Water Conservancy and Water Resources, Hongfeng Road 55., 230088 Hefei, China
[*] Corresponding author, e-mail: guang_liu@hfut.edu.cn

Received: 10 May 2024, Accepted: 10 November 2024, Published online: 19 November 2024

Abstract

To investigate the influence of joints on the segmental lining behavior for a shield tunnel, an analytical model incorporating the effect of the concrete and gaskets is proposed for the segmental joints. Based on the results of the analytical model, a beam-spring numerical model is established for the segmental lining, and parametric studies of the gasket and bolt are conducted to reveal the segmental lining behavior. The numerical results indicate that the joint has a slight influence on the axial force of the segmental lining but significantly affects the bending moment and deformation of the segmental lining. With increasing the gasket thickness or decreasing the gasket hardness, the maximum moment is decreased and the ellipticity is increased, which leads the bending capacity of the segmental lining to be decreased significantly. Therefore, the influence of gaskets should be an indispensable factor during the design of the segmental lining. However, with increasing the bolt pretightening force or the bolt cross-sectional area, the bending capacity of the segmental lining is improved only to a certain extent. Since the ellipticity of the segmental lining is slightly influenced by these bolt parameters, the improvement in the bending capacity can even be neglected.

Keywords

segmental joint, shield tunnel, beam-spring model, rotational stiffness, gasket

1 Introduction

The shield method has been widely used in metro tunnels, highway tunnels, water conveyance tunnels, etc. [1–4]. In the shield tunnel engineering, the longitudinal joint of the segmental lining consists of connecting bolts and some packing materials (e.g., sealing gasket, elastic gasket, etc.), and generally has grooves on its internal and external edges. The joint which has unique geometric constructions and a variety of material interactions is closely related to the safety and stability of segmental lining [5–8].

In some analytical and numerical research, the effect of the segmental joints on the lining behavior is usually considered by indirect methods or direct methods. For the indirect methods, the segmental lining is simulated by a rigid lining ring, and the effect of joints is usually considered by decreasing the rigidity of the lining [9–11]. However, these indirect methods are oversimplified and cannot take the joint stiffnesses or joint distributions into consideration accurately. The direct method generally uses three types of stiffness to model the joint, namely rotational, axial, and shear stiffness [12–15]. Several numerical studies have shown that the axial and shear stiffnesses have a very limited effect on the segmental lining performance [10, 16]. In contrast, segmental lining behavior is largely influenced by the rotational stiffness. It is for this reason that the design of shield tunnels will consider the rotational stiffness as an important parameter. Therefore, the effect of the joint rotational stiffness on the mechanical performance of the segmental lining should be incorporated in the numerical model of the segmental lining behavior.

Based on the direct approach, several numerical studies have uncovered that the higher the rotational stiffness of the joint, the larger the values of the maximum positive and maximum negative bending moments [16, 17]. In these methods, the rotational stiffnesses of the joints are always considered as constants, and the related discussions mainly focus on the influence of different constant values on the lining behavior. However, the experimental and numerical results show that the joint rotational stiffness of shows highly nonlinear characteristics in several stages of the rotational behavior of the joint under the

Cite this article as: Yang, F., Liu, G., Liu, W., Liu, K., Wang, Y., Yao, H. "Modeling the Segmental Lining Behavior Using an Analytical Segmental Joint Model", Periodica Polytechnica Civil Engineering, 69(1), pp. 280–292, 2025. https://doi.org/10.3311/PPci.37309

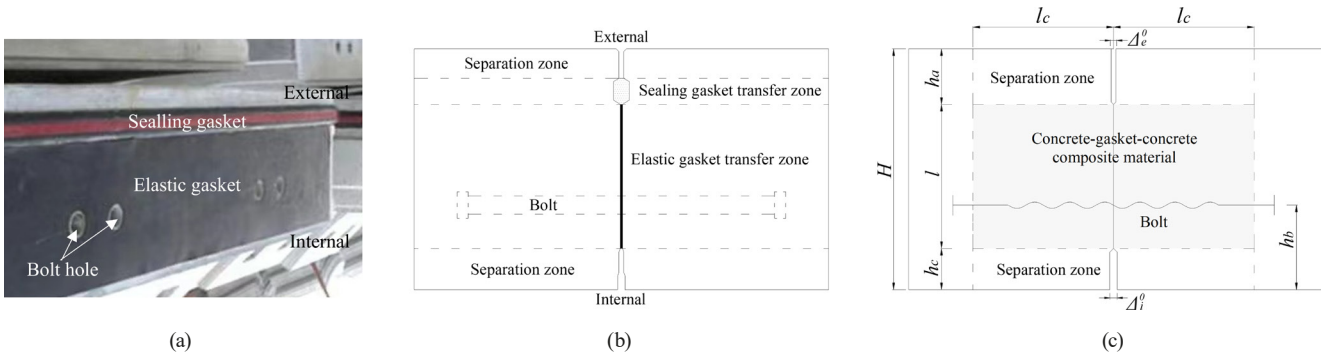

Fig. 1 Modeling assumptions; (a) Segment; (b) Joint details; (c) Assumptions

sagging moment and hogging moment scenarios [18–23]. Besides, some analytical results reveal that some parameters of the bolts and gaskets can affect the joint rotational stiffnesses significantly [23, 24]. Therefore, to investigate the segmental lining behavior, the nonlinear characteristic of the joint rotational stiffnesses should be taken into consideration, and the influence of the bolts and gaskets on the property of the segmental lining should be clarified.

To calculate the joint rotational stiffness, some analytical models have been proposed by establishing equilibrium equations for the axial force and bending moment of the joint contact surface. Typically, the dominant deformation of the longitudinal connection is described by the compressive strain of the concrete and tensile strain of the bolts. The key to these models is the equivalent simulation of the stress distribution shape of the compressed concrete zone which can be equivalent as triangles, combinations, parabolas, etc. [25–30]. In addition to the strains of the concrete and bolt, some analytical solutions also consider the strains of the gaskets, and the results reveal that the joint rotational stiffness is rarely influenced by the sealing gasket but significantly influenced by the elastic gasket [23, 24, 31]. These analytical solutions for the segmental joint with gaskets are proposed based on the assumption that the concrete is much more rigid than the gasket, and the deformations of the gaskets are much greater than that of the concrete. Therefore, only the compressive strains of the gaskets are taken into concertation, and the compressive strains of concrete attached to gaskets are neglected. However, according to the constitutive model of the elastic gasket, the rigidity of the elastic gasket tends to increase rapidly with the increase of compressive stress, and the elastic gasket can no longer be considered as a flexible material in this condition [32–34]. Therefore, when the joints are subject to large moments, the joint rotational stiffnesses calculated by the analytical solutions cannot be in good agreement with the numerical results [24, 31]. The deformations of the gaskets and attached concrete should be both taken into consideration during the calculation of the rotational stiffness of the segmental joint with gaskets.

An improved analytical model is proposed in this study that takes into account the combined effect of concrete and gasket for the segmental lining with gasket. Based on the results of the analytical model, a beam-spring numerical model is established for the segmental lining, and a parametric study of the gaskets and bolts was conducted to investigate the segmental lining performance of the shield tunnel in terms of the main parameters of the joint.

2 Analytical model for the joint rotational behavior

2.1 Modelling assumptions

Fig. 1 presents the details of a typical segmental joint which is equipped with bolts, elastic gaskets and sealing gaskets. According to the condition of the stress transmission, the segmental joint can be classified as a few columnar utilitarian zones. In most cases, the external or internal sides of joints are not contacted in practice unless the joint is subjected to excessive loads [23, 27, 35]. Therefore, the functional zones at the external and internal edges can be assumed as separate zones when the joints are subjected to routine loads. Since the sealing gasket stiffness is much smaller compared to that of the concrete and elastic gaskets, the joint rotational stiffness is rarely influenced by the sealing gasket [23, 24], and the sealing gasket transfer zone can be assumed to be merged into the separation zone. Therefore, the most significant bearing structures of the joint are the bolt and elastic gasket transfer zone. As shown in Fig. 1 (b), the bolt is assumed to be a spring that can only be compressed, but not tensioned, and the elastic gasket transfer zone is assumed as a concrete-gasket-concrete composite columnar.

2.2 Materials model

2.2.1 Concrete

In this model, the multi-linear isotropic hardening behavior is adopted. This stress-strain relationship can be described by Eqs. (1)–(4) [36]:

$$\sigma_c = \begin{cases} f_c\left[1-\left(1-\dfrac{\varepsilon_c}{\varepsilon_0}\right)^n\right] & \left(\varepsilon_c < \varepsilon_0\right) \\ f_c & \left(\varepsilon_0 \le \varepsilon_c \le \varepsilon_{cu}\right) \end{cases}, \tag{1}$$

$$n = 2 - \frac{1}{60}\left(f_{cu,k} - 50\right) \le 2.0, \tag{2}$$

$$\varepsilon_0 = 0.002 + 0.5\times\left(f_{cu,k} - 50\right)\times 10^{-5} \le 0.002, \tag{3}$$

$$\varepsilon_{cu} = 0.0033 - \left(f_{cu,k} - 50\right)\times 10^{-5} \le 0.0033, \tag{4}$$

where σ_c is the compressive stress in the concrete; ε_0 is the strain at the compressive strength (f_c) of the concrete; $f_{cu,k}$ denotes the characteristic value of the concrete compressive strength; ε_{cu} indicates the maximum compressive strain of the concrete.

2.2.2 Bolt

The stress-strain behavior of the bolts is simplified to a bilinear kinematic hardening model with 1% strain hardening after yielding $\left(E_b' = 0.01E_b\right)$, where E_b and E_b' are the elastic and plastic modulus, respectively. The stress-strain relationship can be expressed by the following piecewise function:

$$\sigma_b = \begin{cases} E_b\varepsilon_b & \left(\sigma_b < f_b\right) \\ f_b & \left(\sigma_b \ge f_b\right) \end{cases}, \tag{5}$$

where σ_b and f_b are the stress and yield stress of bolt, respectively.

2.2.3 Gasket

The constitutive model of the elastic gasket can be given by the following equation [33, 34], and the parameter in the equation can be calibrated by the compressive test of the elastic gasket:

$$\sigma_e = E_e\varepsilon_e^{\beta}, \tag{6}$$

where σ_e is the compressive stress when the elastic gasket strain is ε_e, E_e is the similar elastic module, and β is a nonlinear index number.

2.2.4 Composite

According to the materials model of the concrete and elastic gasket, the stress-strain relationship of the concrete-gasket-concrete composite material can be obtained by:

$$\sigma\left(\varepsilon\right) = \sigma_c\left(\varepsilon_c\right) = \sigma_e\left(\varepsilon_e\right), \tag{7}$$

$$\varepsilon = \frac{2\varepsilon_c l_c + \varepsilon_e t}{2l_c + t}, \tag{8}$$

where $\sigma(\varepsilon)$ is the composite stress at any strain ε; as presented in Fig. 1, l_c is the depth of the composite compression zone and roughly equal to the height of the compression zone (l) [23, 27, 35]; t is the thickness of the gasket.

The maximum compressive strain (ε_u) of the composite can be calculated by:

$$\varepsilon_u = \frac{2\varepsilon_{cu} l_c + \varepsilon_{ec} t}{2l_c + t}. \tag{9}$$

2.3 Equilibrium equations

As shown in Fig. 2, the height of the composite compression zone (l) is discretized into n equal sections, and the strains at the two edges are expressed as ε_{e1} and ε_{e2}. Based on the linear strain distribution in Fig. 2, the strain in the center of each section i can be obtained by:

$$\varepsilon_i = \varepsilon_{e1} + \frac{\varepsilon_{e2} - \varepsilon_{e1}}{n}\left(i - 0.5\right). \tag{10}$$

The stress of each section i (σ_i) can be given by the stress-strain behavior of the composite material.

$$\sigma_i = \begin{cases} 0 & \left(\varepsilon_i \le 0\right) \\ \sigma\left(\varepsilon_i\right) & \left(0 < \varepsilon_i \le \varepsilon_u\right) \end{cases} \tag{11}$$

For the joint, from the equilibrium condition of force and moment we have:

$$\sum_{i=1}^{n}\left(\sigma_i\frac{Bl}{n}\right) - nF_b - N = 0, \tag{12}$$

$$\sum_{i=1}^{n}\left(\sigma_i\frac{Bl}{n}\left(\left(b + c - \frac{H}{2}\right) - \frac{l}{n}\left(i - 0.5\right)\right)\right) + nF_b\left(\frac{H}{2} - h_b\right) - M = 0. \tag{13}$$

According to the joint deformation in Fig. 2, the following formula can be obtained:

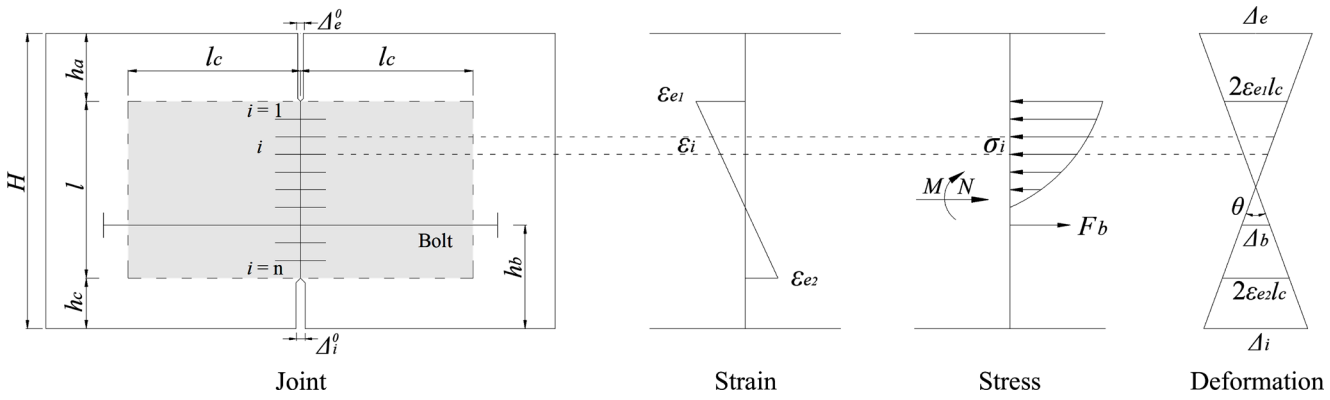

Fig. 2 Modeling approach

$$\frac{2\varepsilon_{e1}l_c - 2\varepsilon_{e2}l_c}{l} = \frac{2\varepsilon_{e1}l_c + \Delta_b}{h_c + l - h_b}, \tag{14}$$

where Δ_b is the joint opening at the bolt. As shown in Eq. (5), the bolt force (F_b) can be calculated by:

$$\varepsilon_b = \frac{\Delta_b}{L_b}, \tag{15}$$

$$F_b = F_0 + A_b\sigma_b, \tag{16}$$

where l_b is the length of the bolt; A_b is the cross-sectional area of the bolt.

Based on the above equations, ε_{e1} and ε_{e2} can be calculated, and the joint rotation angle can be obtained by:

$$\theta = \frac{2\varepsilon_{e1}l_c - 2\varepsilon_{e2}l_c}{l}. \tag{17}$$

Since the concrete contact force at the joint edge is not considered in this study, the joint deformation at the compression edge should meet the following conditions:

$$\Delta_e = 2\varepsilon_{e1}l_c + \theta h_a < \Delta_e^0, \tag{18}$$

$$\Delta_i = 2\varepsilon_{e2}l_c + \theta h_c < \Delta_i^0, \tag{19}$$

where Δ_e is the joint deformation at the compression side for the sagging moment scenario, Δ_e^0 is the beginning gap between the two concrete sections at the outside edge, Δ_i is the joint deformation at the compression edge for the hogging moment scenario, and Δ_i^0 is the beginning gaps between the two concrete sections at the inside edge.

2.4 Verification of the analytical model

2.4.1 Bending test of the segmental joint

As presented in Fig. 3, bending tests of segmented joints were carried out using two connected curved segments [37]. Roller support and fixed support are positioned on the left and right ends of the connected segments,

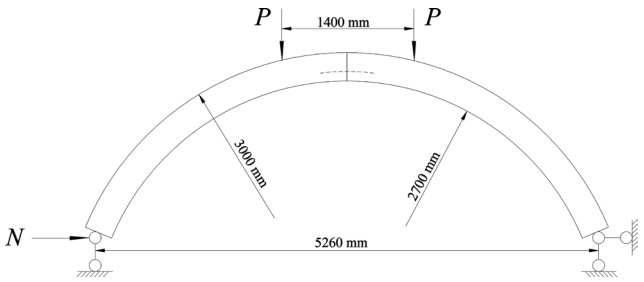

Fig. 3 Sketch view of the bending test

respectively. During the loading process, the eccentricity (e) is fixed to 100 mm, the horizontal loads (N) and vertical loads (P) increase gradually, and joint deformations are observed.

The joint rotation angle (θ) illustrated in Fig. 4 can be calculated by Eq. (20). The rotational stiffness of the joint can be thought of as the slope of the joint rotation angle versus the bending moment curve.

The joint rotation angle (θ) illustrated in Fig. 4 can be calculated by Eq. (20). The rotational stiffness of the joint can be thought of as the slope of the joint rotation angle versus the bending moment curve:

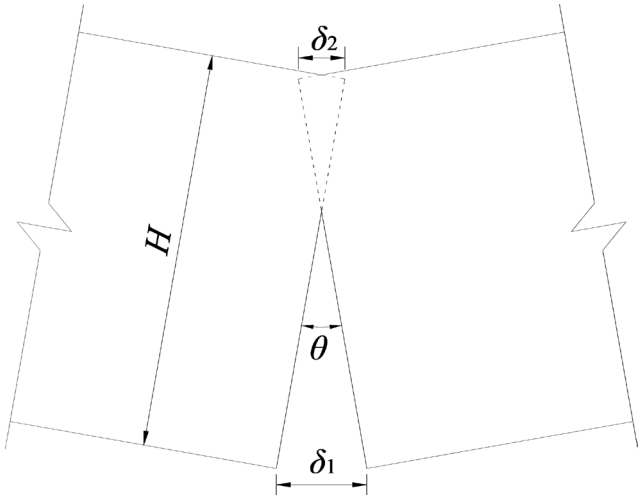

Fig. 4 Sketch view of the joint rotation angle

$$\theta = \frac{\delta_1 - \delta_2}{H}, \tag{20}$$

where δ_1 and δ_2 are the averaged deformation at the opening and compression sides, respectively, and H is the thickness of the segment.

2.4.2 Comparison between the analytical results and experimental results

The dimensions and materials related to the segmental joint in the experiment are listed as follows:

1. Segment and joint: B = 1200 mm, H = 300 mm, h_a = 80 mm, h_b = 120 mm, h_c = 40 mm, l = 180 mm;
2. Concrete: type C50, f_c = 32.4 MPa;
3. Bolt: E_b = 210 GPa, f_b = 640 MPa, L_b = 431 mm, A_b = 452.2 mm^2, n = 2, F_0 = 20 kN;
4. Elastic gasket: E_e = 2480 MPa; β = 1.67; t = 4 mm for the sagging moment scenario; t = 6 mm for the hogging moment scenario.

The stress and strain of the concrete-gasket-concrete composite material in the analytical model can be calculated using Eqs. (7) and (8). As presented in Fig. 5, it is obvious that the composite is much softer than the concrete. That means the elastic gaskets have a significant effect of softening the joint, and with the increase of the gasket thickness, this effect tends to be more obvious. Therefore, the elastic gasket, which is an important part of the joint, should be reflected in the calculation of the rotational stiffness.

Applying an axial force to the joint, the rotation angle of joint can be estimated using proposed analytical model. According to the analytical results in Fig. 6, in the condition that the eccentricity (e) is fixed to 100 mm, with the axial force increasing constantly, the joint rotation angles for the sagging moment scenario and hogging moment scenario both tend to increase obviously. The experimental results

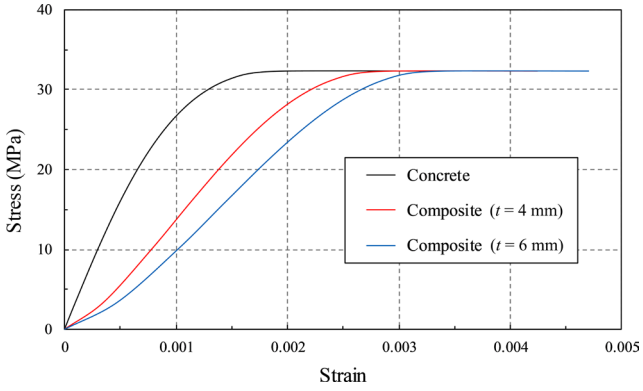

Fig. 5 Stress-strain behavior for the composite

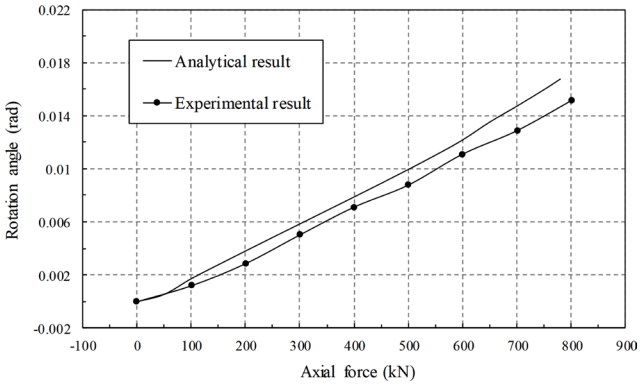

(a)

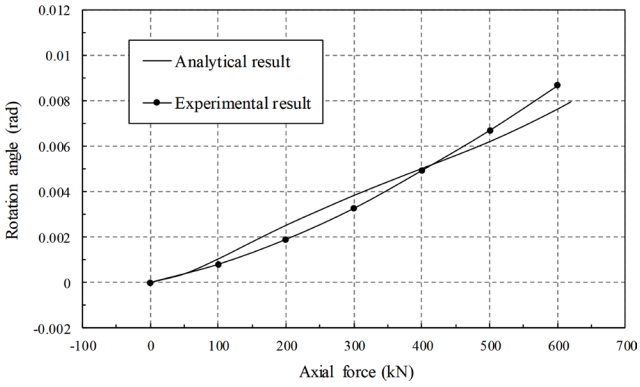

(b)

Fig. 6 Comparison between analytical results and experimental results; (a) Sagging moment scenario; (b) Hogging moment scenario

are also presented in Fig. 6 for comparison. According to the comparison, the curves from the proposed analytical model are well consistent with that from the experimental results, and the proposed analytical model for the joint rotation stiffness is verified.

3 Segmental tunnel lining behavior

3.1 Study case of the Yellow River Crossing Tunnel

To investigate the behavior of the segmental lining, the Yellow River Crossing Tunnel is studied as a case. As shown in Fig. 7 (a), one segment ring of the lining consists of 7 segments. The segment external radius is 4350 mm, the internal radius is 3950 mm, and the width is 1600 mm. To strictly control the tunnel deformation, prepoured sections are quickly installed in designated locations to resist possible earth and external water pressures after excavation. The loads of the normal operation condition are presented in Fig. 7 (b), and the external water pressure in the tunnel center is 0.32 MPa.

The dimensions and materials related to the segmental joint of the lining are listed as follows:

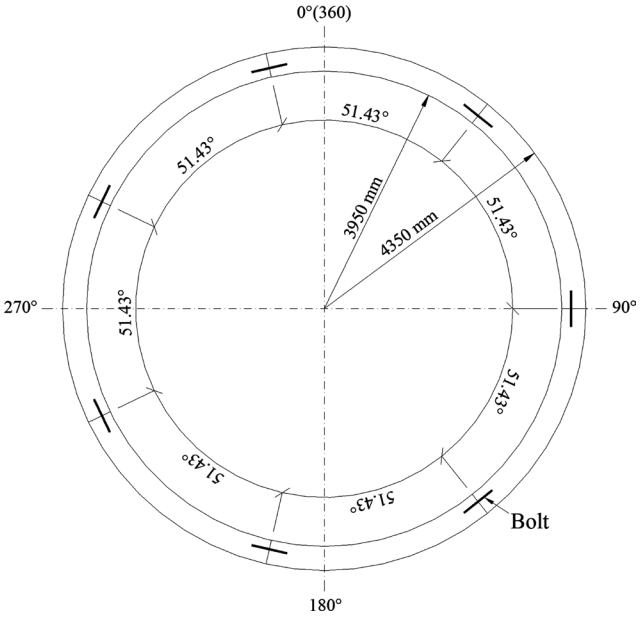

(a)

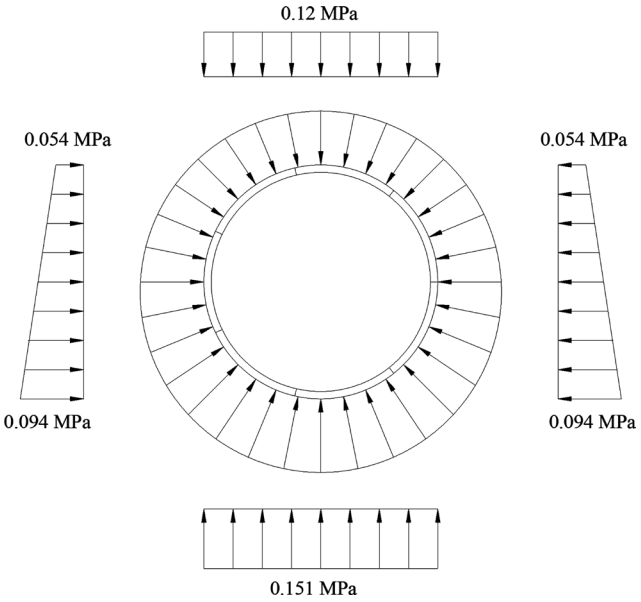

(b)

Fig. 7 Segmental ling of the Yellow River Crossing Tunnel; (a) Segments arrangement; (b) Loading condition

1. Segment and joint: B = 1600 mm, H = 400 mm, h_a = 104 mm, h_b = 150 mm, h_c = 25 mm, l = 271 mm;
2. Concrete: type C50, f_c = 32.4 MPa;
3. Bolt: E_b = 210 GPa, f_b = 480 MPa, L_b = 600 mm, A_b = 706.5 mm^2, n = 4, F_0 = 100 kN;
4. Elastic gasket: E_e = 378.39 MPa; β = 3.0892; t = 1.5 mm.

3.2 Numerical model of the segmental lining

As shown in Fig. 8, a 2D beam-spring numerical model is established for the segmental lining. The segment is

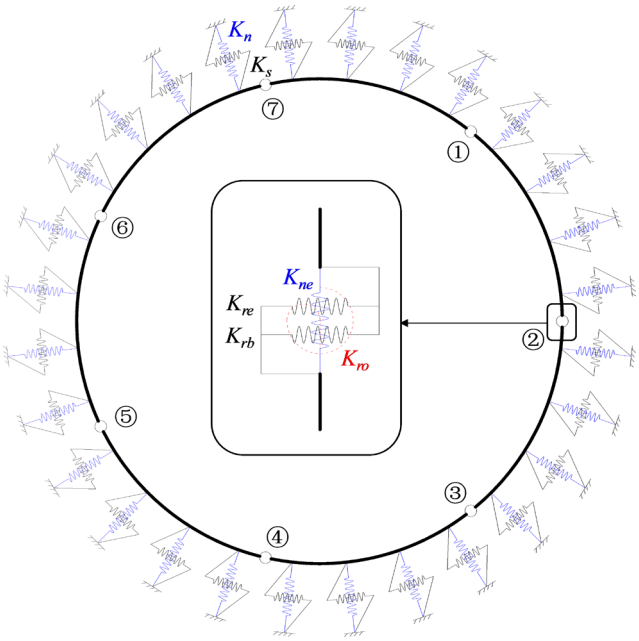

Fig. 8 Beam-spring numerical model of the segmental lining

modeled by the beam element, and the joint is modeled by a set composed of a rotational spring (K_{ro}), an axial spring (K_{ne}), and two radial springs (K_{re} and K_{rb}). The ground-structure interaction is modeled by two springs: one normal spring (K_n) and one shear spring (K_s). Normal springs can withstand compressive loads, not tensile loads are introduced in the model to capture the ground-structure interaction.

For the ground-structure interaction springs, the stiffnesses can be calculated by the following equations [38–40]:

$$K_n = \frac{E}{R(1+\mu)} A_s, \tag{21}$$

$$K_s = \frac{1}{3} K_n, \tag{22}$$

where E is the soil elastic modulus; R is the tunnel radius; μ is the Poisson ratio; A_s is the area corresponding to a single spring.

For the segmental joint springs, the axial spring (K_{ne}) represents the compression effect of the elastic gasket, and the spring stiffness can be obtained by Eq. (6). The radial spring (K_{re}) represents the shear effect of the elastic gasket. The shear stress versus shear strain relationship ($\tau_e(\gamma_e)$) of the elastic gasket is given by the experimental results [32], and the spring stiffness can be obtained by:

$$F_{re} = \tau_e(\gamma_e) \times A_e, \tag{23}$$

$$\gamma_e = \frac{D_{re}}{t}, \tag{24}$$

where F_{re} is the spring force; τ_e indicates the shear stress of the elastic gasket; γ_e denotes the shear strain of the elastic gasket; A_e is the shear area of the elastic gasket; D_{re} is spring shear deformation.

The radial spring (K_{rb}) represents the shear effect of the bolt, and the spring stiffness can be obtained by:

$$F_{rb} = nG_b \frac{D_{rb}}{l_b} A_b, \tag{25}$$

where F_{rb} is the spring force; G_b is the bolt shear modulus; D_{rb} is the spring shear deformation.

The rotational spring (K_{ro}) represents the rotational behavior of the segmental joint, and the spring stiffness can be calculated by the proposed analytical model in Section 2. To calculate the rotational stiffnesses of the joints subjected to different axial forces, a continuous beam model is established for the segmental lining, and the force and moment corresponding to the joint positions are estimated. According to the estimation, the axial forces of the joints ①, ③, ④ and ⑦ are about 3000 kN, and these joints are subjected to sagging moments. The axial forces of the joints ⑤ and ⑥ are about 3200 kN, the axial force of the joint ② is about 3500 kN, and these joints are subjected to hogging moments. Besides, the estimated maximum sagging moment of the lining does not exceed 300 kN m, and the estimated maximum hogging moment of the lining does not exceed 400 kN m. It can be seen from Fig. 9 that the rotational stiffness of each joint is the slope of the joint rotation angle versus the bending moment curve.

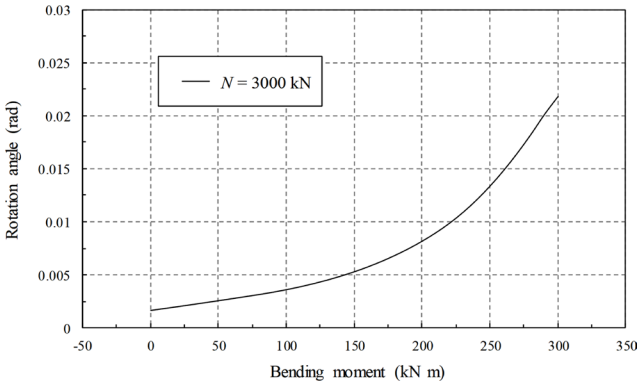

(a)

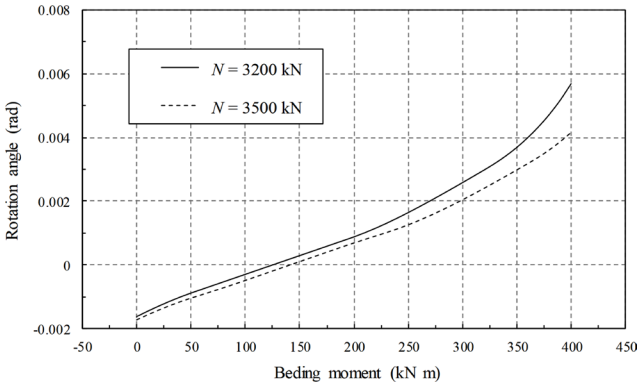

(b)

Fig. 9 Variation of the joint rotation angle with bending moment; (a) Sagging moment scenario; (b) Hogging moment scenario

3.3 Results and discussion

The axial forces, bending moments and deformations of the segmental lining calculated by the beam-spring model and continuous beam model are presented in Fig. 10. Fig. 10 (a) indicates that the joint has limited influence on the axial force of the segmental lining. The differences of the calculated axial forces between the two models are within 3%. However, Fig. 10 (b) and Fig. 10 (c) indicate that the joint has a significant influence on the bending moments and deformations of the segmental lining. With the influence of the joint, the maximum sagging moment decreases by 70.4%, and the maximum hogging moment decreases by 23.5%. Referring to the code of shield tunneling method GB 50446-2017 [41], the deformation degree of the lining can be characterized by ellipticity (λ_e) which can be calculated by:

$$\lambda_e = \frac{D_{\max} - D_{\min}}{D}, \tag{26}$$

where D is the diameter of the undeformed lining; $D_{\max}$ is the maximum diameter of the deformed lining; $D_{\min}$ is the minimum diameter of the deformed lining. According to the deformation results, with the influence of the joint, the ellipticity increases by 51.6%.

3.4 Parametric study

3.4.1 Influence of the gasket thickness

Under the same load, the segmental lining bending moment and deformation vary with the change of elastic gasket thickness. To address this issue, we designed several examples to calculate the bending moment and deformation of the segmental lining with different gasket thicknesses of 1 mm, 1.5 mm and 2 mm. As shown in Fig. 12, with the increase of the gasket thickness from 1 mm to 2 mm, the maximum sagging moment decreases by 20.1%, the maximum hogging moment decreases by 14.9%, and the ellipticity increases by 11.8%.

According to Eqs. (7) and (8), the gasket thickness affects the constitutive relation of the concrete-gasket-concrete composite material directly. Since the concrete-gasket-concrete composite is the important bearing

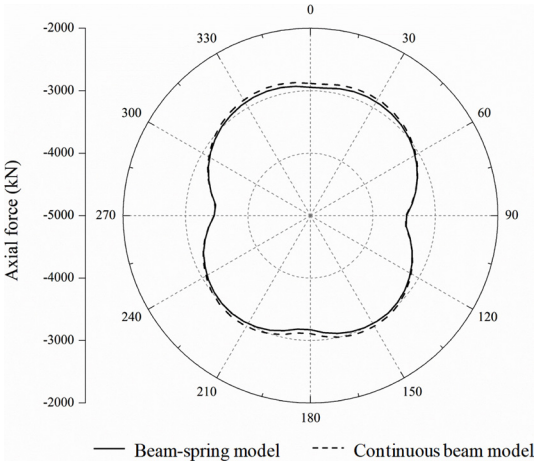

(a)

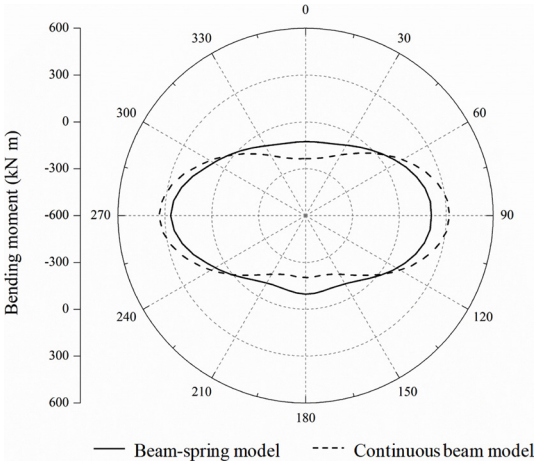

(b)

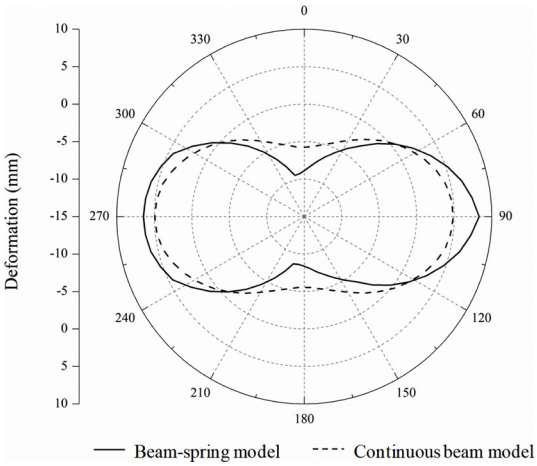

(c)

Fig. 10 Comparison between the beam-spring model results and continuous beam model results; (a) Axial force; (b) Bending moment; (c) Deformation

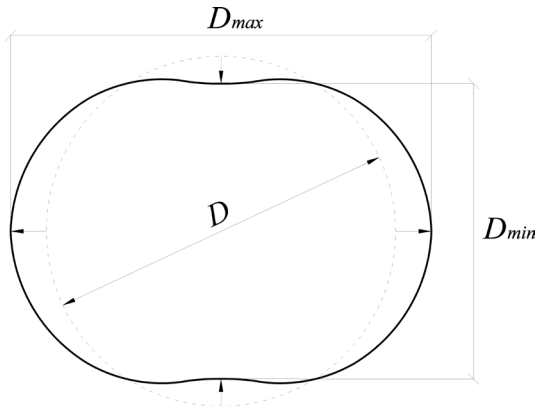

Fig. 11 Sketch view of the lining deformation

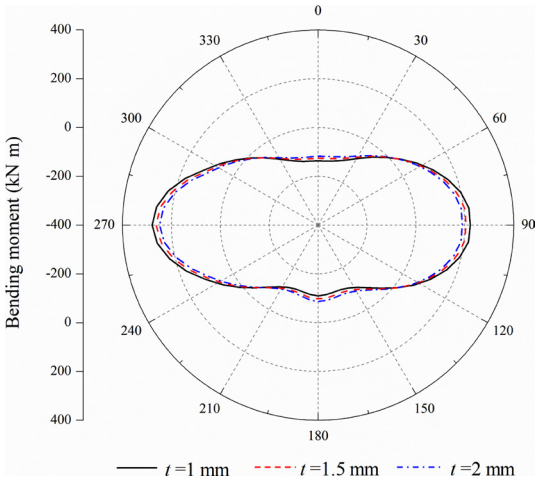

(a)

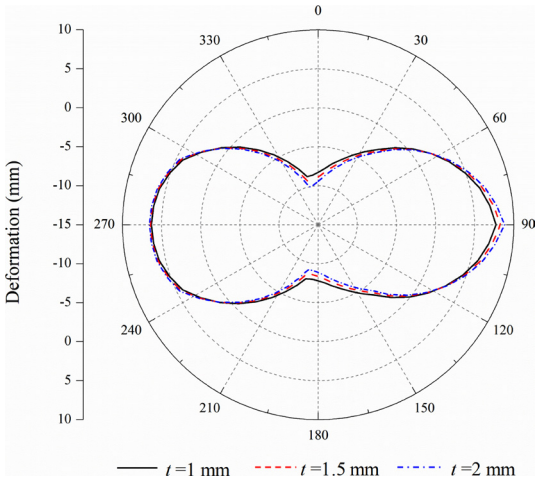

(b)

Fig. 12 Variations of the bending moment and deformation with the gasket thickness; (a) Bending moment; (b) Deformation

structure for the segmental joint, the physical mechanism of elastic gasket thickness effect on segmental liner performance requires to be revealed. Figs. 5 and 12 manifest that the elastic gaskets can soften the joint, i.e., reduction in the stiffness of the joints. With the increase of the gasket thickness, this softening tends to be more obvious, and the bending capacity of the segmental lining is decreased,

which leads to decreased bending moments and increased deformations for the segmental lining.

3.4.2 Influence of the gasket hardness

According to some experimental results, the constitutive model of the elastic gasket is complex and diverse [32–34]. The bending moments and the deformations of the segmental lining with different gasket hardness of hard $\left(\sigma_e = 1892.0\varepsilon_e^{3.1}\right)$, moderate $\left(\sigma_e = 378.4\varepsilon_e^{3.1}\right)$, soft $\left(\sigma_e = 75.7\varepsilon_e^{3.1}\right)$ are calculated to investigate the impact of the elastic gasket hardness on the segmental lining performance. Fig. 13 indicates that, with the decrease of the gasket hardness from hard to soft, the maximum sagging moment decreases by 29.8%, the maximum hogging moment decreases by 22.5%, and the ellipticity increases by 20.3%.

As shown in Fig. 1, the gasket and concrete together form the load-bearing structure of the joint. Therefore, the change in gasket hardness directly affects the stress and deformation of the concrete-gasket-concrete composite. This variation in the stress-strain relationship of the composite further produces different segmental lining behaviors. Similarly, with the decrease of the gasket hardness, this softening effect of the gasket on the segmental joint tends to be more obvious, and the bending capacity of the segmental lining is decreased, which leads the bending moments to be decreased and the deformations to be increased for the segmental lining.

3.4.3 Influence of the bolt pretightening force

To investigate the influence of the bolt pretightening force (F_0) on the segmental lining behavior, the bending moments and the deformations of the segmental lining with different bolt pretightening forces of 0 kN, 50 kN, 100 kN and 150 kN are calculated. As presented in Fig. 14, with the increase of the pretightening force from 0 to 150 kN, the maximum sagging moment increases by 19.6%, the maximum hogging moment increases by 10.1%, and the ellipticity decreases by only 4.4%.

Fig. 14 indicates that, with the increase of the bolt pretightening force, the bending capacity of the segmental lining is improved, which leads to increased bending moments and decreased deformations for the segmental lining. However, compared with the axial force of the segmental joint and the resultant force of the concrete-gasket-concrete composite, the bolt pretightening force is much smaller. Therefore, according to Eqs. (12) and (13), the bolt pretightening force can affect the lining behavior but only to a certain extent, especially for the lining deformation which is rarely influenced by the bolt pretightening force.

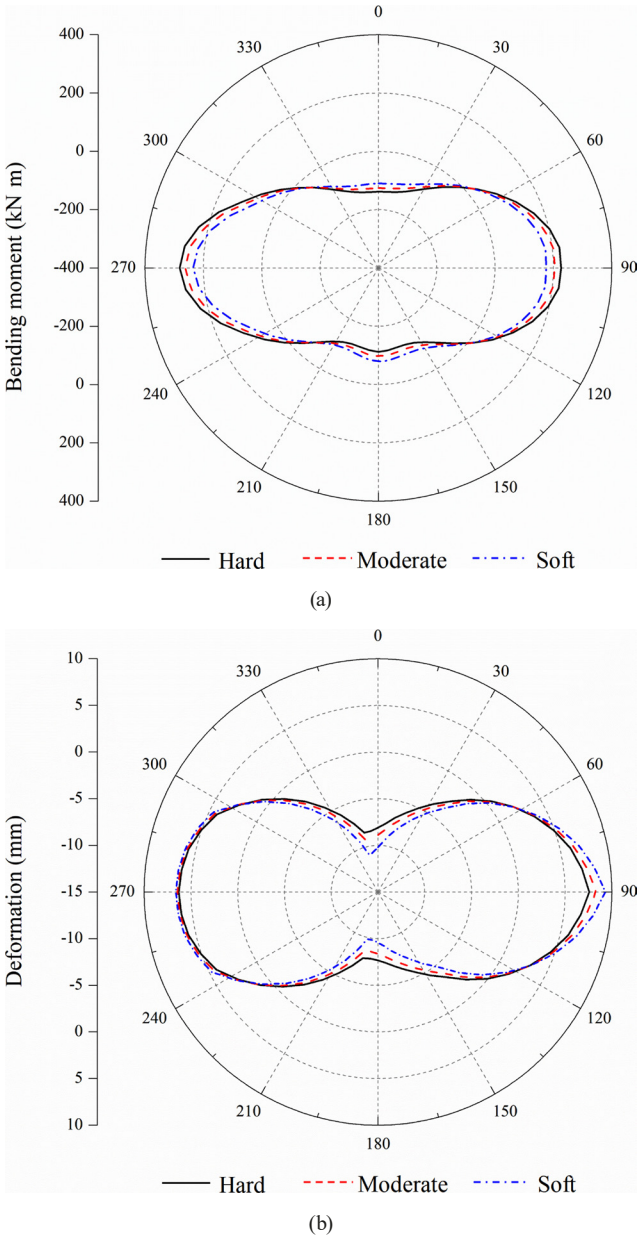

Fig. 13 Variations of the bending moment and deformation with the gasket hardness; (a) Bending moment; (b) Deformation

3.4.4 Influence of the bolt type

The bending moments and the deformations of the segmental lining with different bolt types of M27 (A_b = 572.3 mm^2), M30 (A_b = 706.5 mm^2), M33 (A_b = 854.9 mm^2) and M36 (A_b = 1017.4 mm^2) are calculated to investigate the influence of the bolt type on the segmental lining behavior. As shown in Fig. 15, with the increase of the bolt cross-sectional area from 572.3 mm^2 to 1017.4 mm^2, the maximum sagging moment increases by only 3.2%, the maximum

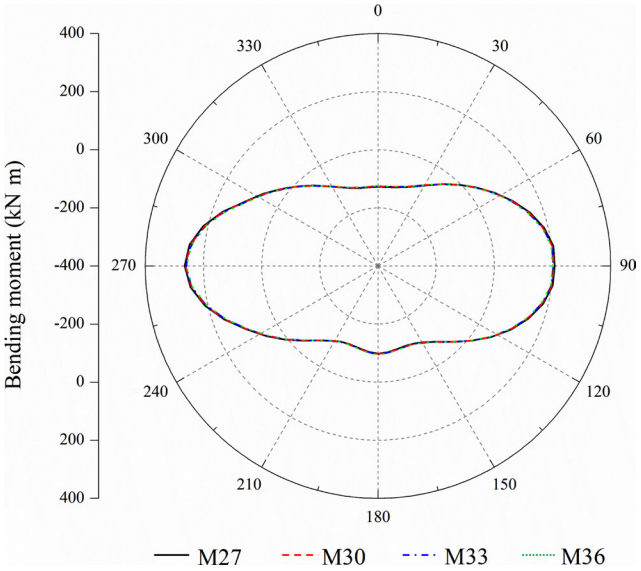

(a)

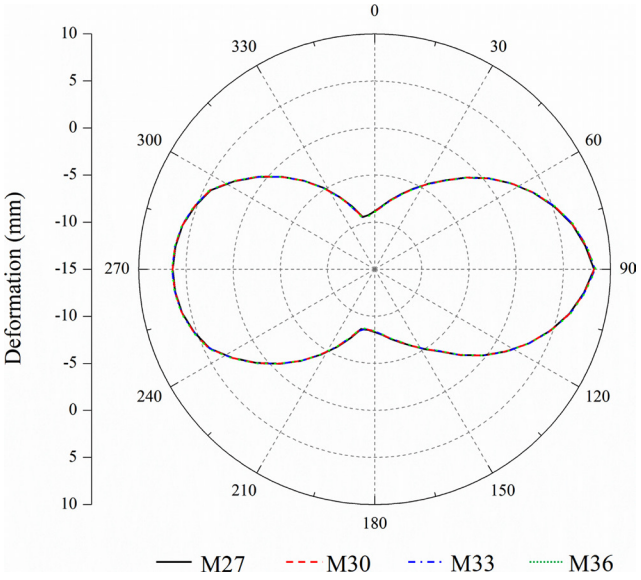

(b)

Fig. 14 Variations of the bending moment and deformation with the bolt pretightening forces; (a) Bending moment; (b) Deformation

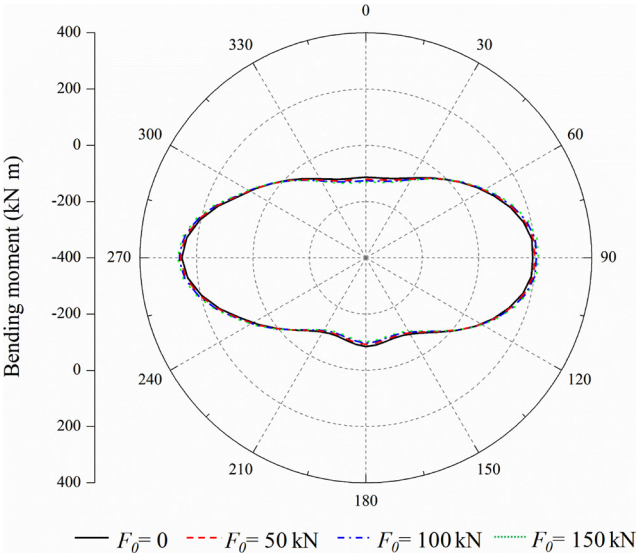

(a)

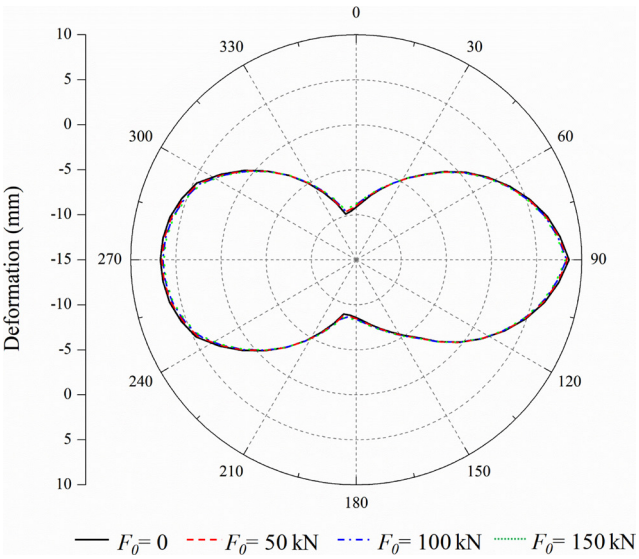

(b)

Fig. 15 Variations of the bending moment and deformation with the bolt cross-sectional area; (a) Bending moment; (b) Deformation

hogging moment increases by only 3.6%, and the ellipticity decreases by only 1.4%.

As shown in Fig. 15, with the increase of the bolt cross-sectional area, the bending moments go up, and the deformations decline, which implies that the bending capacity of the segmental lining improved. However, since the joint opening is very small when the lining is subject to the routine loads, the bolts are not significantly tensioned. Compared with the axial force of the segmental joint and the resultant force of the concrete-gasket-concrete composite, the bolt force is much smaller. Therefore, the increase of the bolt cross-sectional area can improve the bending capacity of the segmental lining only to a certain extent. However, the enhancement in the bending capacity can largely be ignored, for the reason that the increased maximum bending moments and the decreased ellipticity are all within 4%.

4 Conclusions

An improved analytical model that incorporates the effect of the concrete and gaskets is proposed in this research for the segmental joint rotational behavior. Based on the rotational stiffness calculated by the analytical model, a beam-spring numerical model is established for the segmental lining to investigate the influence of the joint on

the segmental lining behavior, and the following conclusions can be drawn.

The concrete-gasket-concrete composite acting as a primary load-bearing structure is common in segmental joints with gaskets. The proposed analytical model for the segmental joint, which is verified by the experimental results, can take the combined work of the concrete and gasket into consideration, and the complex nonlinear characteristic of the joint rotational stiffnesses can be calculated. It is a simplified and feasible method to figure up the rotational stiffness of the concrete-gasket-concrete composite in the segmental joint.

The elastic gasket located between the concrete structures has a significant effect of softening the segmental joint, and with the increase of the gasket thickness, this effect tends to be more obvious. Since it plays an important role in the joint rotational behavior, it should not be neglected during the design of the segmental joint, including calculating the joint rotational stiffnesses and analyzing the influence of the joint component on the segmental lining performance.

Based on the analytical model for the joint, the joint rotational stiffnesses can be obtained and simulated by the rotational spring of the beam-spring model established for the segmental lining. The numerical results indicate that the joint has a small influence on the axial forces of the segmental lining but significantly affects the bending moments and deformations of the segmental lining. With the influence of the joint, the maximum sagging moment decreases by 70.4%, the maximum hogging moment decreases by 23.5%, and the ellipticity increases by 51.6%.

With the increase of the gasket thickness from 1 mm to 2 mm, the maximum sagging moment decreases by 20.1%, the maximum hogging moment decreases by 14.9%, and the ellipticity increases by 11.8%. With the decrease of the gasket hardness from hard $\left(\sigma_e = 1892.0\varepsilon_e^{3.1}\right)$ to soft $\left(\sigma_e = 75.7\varepsilon_e^{3.1}\right)$, the maximum sagging moment decreases by 29.8%, the maximum hogging moment decreases by 22.5%, and the ellipticity increases by 20.3%. Therefore, the gasket has a significant influence on the segmental lining behavior. With the increase of the gasket thickness or the decrease of the gasket hardness, the bending capacity of the segmental lining is decreased obviously.

When the pretightening force rises from 0 to 150 kN, the maximum sagging moment increases by 19.6%, the maximum hogging moment increases by 10.1%, and the ellipticity decreases by only 4.4%. As the bolt cross-sectional area changes from 572.3 mm^2 to 1017.4 mm^2, the maximum sagging moment increases by only 3.2%, the maximum hogging moment increases by only 3.6%, and the ellipticity decreases by only 1.4%. Therefore, the increase of the bolt pretightening force and the bolt cross-sectional area can improve the bending capacity of the segmental lining only to a certain extent. However, this improvement can even be neglected because the decreased ellipticity of the segmental lining caused by the increase of the bolt pretightening force and the bolt cross-sectional area are both within only 5%.

In sum, for the segmental lining under normal operation conditions, the joint elastic gasket has an even greater impact than the bolt on the lining bending capacity, and the combined effect of the concrete and gasket should be fully taken into account during the calculation of the joint rotational stiffness and analysis of the overall lining performance.

Acknowledgment

This work was supported by Anhui Provincial Natural Science Foundation (2308085QE194), and Anhui Province Key Laboratory of Water Conservancy and Water Resources (2023SKJ05).

References

[1] Ren, D.-J., Shen, S.-L., Arulrajah, A., Wu, H.-N. "Evaluation of ground loss ratio with moving trajectories induced in double-O-tube (DOT) tunnelling", Canadian Geotechnical Journal, 55(6), pp. 894–902, 2018. https://doi.org/10.1139/cgj-2017-0355

[2] Eftekhari, A., Aalianvari, A. "An overview of several techniques employed to overcome squeezing in mechanized tunnels; A case study", Geomechanics and Engineering, 18(2), pp. 215–224, 2019. https://doi.org/10.12989/gae.2019.18.2.215

[3] Bui, H.-G., Ninić, J., Koch, C., Hackl, K., Meschke, G. "Integrated BIM-based modeling and simulation of segmental tunnel lining by means of isogeometric analysis", Finite Elements in Analysis and Design, 229, 104070, 2024. https://doi.org/10.1016/j.finel.2023.104070

[4] Babanagar, N., Sheil, B., Ninić, J., Zhang, Q., Hardy, S. "Digital twins for urban underground space", Tunnelling and Underground Space Technology, 155, 10614, 2025. https://doi.org/10.1016/j.tust.2024.106140

[5] Huang, M., Shi, X., Yang, F., Liu, K. "Numerical Investigation for the Bearing Performance of the Segmental Joint with Elastic Gasket", Periodica Polytechnica Civil Engineering, 66(4), pp. 1158–1168, 2022. https://doi.org/10.3311/PPci.20058

[6] Lorenzo, S. G. "The role of temporary spear bolts in gasketed longitudinal joints of concrete segmental linings", Tunnelling and Underground Space Technology, 105, 103576, 2020. https://doi.org/10.1016/j.tust.2020.103576

[7] Wu, H.-N., Shen, S.-L., Chen, R.-P., Zhou, A. "Three-dimensional numerical modelling on localised leakage in segmental lining of shield tunnels", Computres and Geotechnics, 122, 103549, 2020. https://doi.org/10.1016/j.compgeo.2020.103549

[8] Zaheri, M., Ranjbarnia, M., Dias, D. "3D numerical investigation of segmental tunnels performance crossing a dip-slip fault", Geomechanics and Engineering, 23(4), pp. 351–364, 2020. https://doi.org/10.12989/gae.2020.23.4.351

[9] Duddeck, H., Erdmann, J. "Structural design models for tunnels: Tunnelling 82, proceedings of the 3rd international symposium, Brighton, 7–11 June 1982, P83–91. Publ London: IMM, 1982", International Journal of Rock Mechanics and Mining Sciences & Geomechanics Abstracts, 20(1), A15, 1983. https://doi.org/10.1016/0148-9062(83)91736-9

[10] Working Group No. 2, International Tunnelling Association "Guidelines for the design of shield tunnel lining", Tunnelling and Underground Space Technology, 15(3), pp. 303–331, 2020. https://doi.org/10.1016/S0886-7798(00)00058-4

[11] Lee, K. M., Ge, X. W. "The equivalence of a jointed shield-driven tunnel lining to a continuous ring structure", Canadian Geotechnical Journal, 38(3), pp. 461–483, 2001. https://doi.org/10.1139/cgj-38-3-461

[12] Lee, K. M., Hou, X. Y., Ge, X. W., Tang, Y. "An analytical solution for a jointed shield-driven tunnel lining", International Journal for Numerical and Analytical Methods in Geomechanics, 25(4), pp. 365–390, 2001. https://doi.org/10.1002/nag.134

[13] Ding, W. Q., Yue, Z. Q., Tham, L. G., Zhu, H. H., Lee, C. F., Hashimoto, T. "Analysis of shield tunnel", International Journal for Numerical and Analytical Methods in Geomechanics, 28(1), pp. 57–91, 2004. https://doi.org/10.1002/nag.327

[14] Do, N.-A., Dias, D., Oreste, P., Djeran-Maigre, I. "Three-dimensional numerical simulation for mechanized tunnelling in soft ground: the influence of the joint pattern", Acta Geotechnica, 9(4), pp. 673–694, 2014. https://doi.org/10.1007/s11440-013-0279-7

[15] Nematollahi, M., Molladavoodi, H., Dias, D. "Three-dimensional numerical simulation of the Shiraz subway second line – influence of the segmental joints geometry and of the lagging distance between twin tunnels' faces", European Journal of Environmental and Civil Engineering, 24(10), pp. 1606–1622, 2020. https://doi.org/10.1080/19648189.2018.1476270

[16] Do, N.-A., Dias, D., Oreste, P., Djeran-Maigre, I. "2D numerical investigation of segmental tunnel lining behavior", Tunnelling and Underground Space Technology, 37, pp. 115–127, 2013. https://doi.org/10.1016/j.tust.2013.03.008

[17] Teachavorasinskun, S., Chub-uppakarn, T. "Influence of segmental joints on tunnel lining", Tunnelling and Underground Space Technology, 25(4), pp. 490–494, 2010. https://doi.org/10.1016/j.tust.2010.02.003

[18] Zhu, H., Huang, B., Li, X., Hashimoto, T. "盾构衬砌管片接头内力-变形统一模型及试验分析" (Unified model for internal force and deformation of shield segment joints and experimental analysis), Chinese Journal of Geotechnical Engineering, 36(12), pp. 2153–2160, 2014. (in Chinese) https://doi.org/10.11779/CJGE201412001

[19] Feng, K., He, C., Qiu, Y., Zhang, L., Wang, W., Xie, H., Zhang, Y., Cao, S. "Full-scale tests on bending behavior of segmental joints for large underwater shield tunnels", Tunnelling and Underground Space Technology, 75, pp. 100–116, 2018. https://doi.org/10.1016/j.tust.2018.02.008

[20] Jamshidi Avanaki, M., Hoseini, A., Vahdani, S., de la Fuente, A. "Numerical-aided design of fiber reinforced concrete tunnel segment joints subjected to seismic loads", Construction and Building Materials, 170, pp. 40–54, 2018. https://doi.org/10.1016/j.conbuildmat.2018.02.219

[21] Kavvadas, M., Litsas, D., Vazaios, I., Fortsakis, P. "Development of a 3D finite element model for shield EPB tunnelling", Tunnelling and Underground Space Technology, 65, pp. 22–34, 2017. https://doi.org/10.1016/j.tust.2017.02.001

[22] Matsumoto, Y., Wakui, I., Tamamatsu, J., Iwanami, M. "Structural analysis model of joints in steel segment shield tunnel for 3D FEM", In: Anagnostou, G., Benardos, A., Marinos, V. P. (eds.) Expanding Underground - Knowledge and Passion to Make a Positive Impact on the World, CRC Press, 2023, pp. 735–742. ISBN 9781003348030 https://doi.org/10.1201/9781003348030-89

[23] Li, X., Yan, Z., Wang, Z., Zhu, H. "Experimental and analytical study on longitudinal joint opening of concrete segmental lining", Tunnelling and Underground Space Technology, 46, pp. 52–63, 2015. https://doi.org/10.1016/j.tust.2014.11.002

[24] Yang, F., Cao, S., Li, Q. "An analytical model for the rotational behavior of concrete segmental lining longitudinal joints with gaskets", Advances in Structural Engineering, 22(13), pp. 2866–2881, 2019. https://doi.org/10.1177/1369433219852566

[25] Koyama, Y. "Study on the Improvement of Design Method of Segments for Shield-driven Tunnels", RTRI Report, 33, pp. 47–55, 2000.

[26] Shen, Y., Yan, Z., Zhu, H. "An Analytical Mechanical Model for Tunnel Segmental Joints Subjected to Elevated Temperatures", In: Zhao, S., Liu, J., Zhang, X. (eds.) Innovative Materials and Design for Sustainable Transportation Infrastructure, ASCE Press, 2015, pp. 329–340. ISBN 9780784479278 https://doi.org/10.1061/9780784479278.031

[27] Tvede-Jensen, B., Faurschou, M., Kasper, T. "A modelling approach for joint rotations of segmental concrete tunnel linings", Tunnelling and Underground Space Technology, 67, pp. 61–67, 2017. https://doi.org/10.1016/j.tust.2017.04.019

[28] Marwan, A., Gall, V. E., Alsahly, A., Meschke, G. "Structural forces in segmental linings: process-oriented tunnel advance simulations vs. conventional structural analysis", Tunnelling and Underground Space Technology, 111, 103836, 2021. https://doi.org/10.1016/j.tust.2021.103836

[29] Majdi, A., Ajamzadeh, H., Nadimi, S. "Investigation of moment-rotation relation in different joint types and evaluation of their effects on segmental tunnel lining", Arabian Journal of Geosciences, 9(7), 512, 2016. https://doi.org/10.1007/s12517-016-2538-z

[30] Do, N. A., Dias, D., Oreste, P. "Simplified approach to the design of segmental tunnel linings", Proceedings of the Institution of Civil Engineers - Geotechnical Engeering, 171(3), pp. 209–214, 2018. https://doi.org/10.1680/jgeen.17.00088

[31] Yang, F., Cao, S., Qin, G. "Simplified spring models for concrete segmental lining longitudinal joints with gaskets", Tunnelling and Underground Space Technology, 96, 103227, 2020. https://doi.org/10.1016/j.tust.2019.103227

[32] Cavalaro, S. H. P., Aguado, A. "Packer behavior under simple and coupled stresses", Tunnelling and Underground Space Technology, 28, pp. 159–173, 2012. https://doi.org/10.1016/j.tust.2011.10.008

[33] Xiaochun, Z., Wei, Z., Zhengrong, H., Yuewang, H. "Effect of joint structure on joint stiffness for shield tunnel lining", Tunnelling and Underground Space Technology, 21(3–4), pp. 407–408, 2006. https://doi.org/10.1016/j.tust.2005.12.215

[34] Zhang, J., He, C. "不同承压衬垫的管片接头力学性能分析" (Analysis on mechanical properties of segment joints with different pressure pads), Journal of Chinese Railway Society, 35(12), pp. 101–105, 2013. (in Chinese) https://doi.org/10.3969/j.issn.1001-8360.2013.12.016

[35] Janssen, P. "Tragverhalten von Tunnelausbauten mit Gelenktübbings" (Load-bearing behavior of tunnel extensions with articulated segments), PhD thesis, Technische Universität Braunschweig, 1983.

[36] National Standard of the People's Republic of China "GB 50010-2010 混凝土结构设计规范" (GB 50010-2010 Code for Design of Concrete Structures), China Architecture & Building Press, Beijing, China, 2010. (in Chinese)

[37] Zhou, H., Chen, T., Li, L. "地铁区间盾构隧道衬砌接头的荷载试验" (Study on joint load test of metro shield tunneling lining), Industrial Construction, 40(4), pp. 79–83, 2010. (in Chinese) https://doi.org/10.13204/j.gyjz2010.04.001

[38] Do, N. A., Dias, D., Zhang, Z., Huang, X., Nguyen, T. T., Pham, V. V., Nait-Rabah, O. "Study on the behavior of squared and sub-rectangular tunnels using the Hyperstatic Reaction Method", Transportation Geotechnics, 22, 100321, 2020. https://doi.org/10.1016/j.trgeo.2020.100321

[39] Arnau, O., Molins, C. "Three dimensional structural response of segmental tunnel linings", Engineering Structures, 44, pp. 210–221, 2012. https://doi.org/10.1016/j.engstruct.2012.06.001

[40] Miao, Y., Yao, E., Ruan, B., Zhuang, H. "Seismic response of shield tunnel subjected to spatially varying earthquake ground motions", Tunnelling and Underground Space Technology, 77, pp. 216–226, 2018. https://doi.org/10.1016/j.tust.2018.04.006

[41] National Standard of the People's Republic of China "GB 50446-2017 盾构法隧道施工与验收规范" (GB 50446-2017 Code for Construction and Acceptance of Shield Tunnelling Method), China Architecture & Building Press, Beijing, China, 2017. (in Chinese)